A numerical procedure to test the effects of the main variables in the submerged arc welding process

CONTE Romina[1,a *], RODRÌGUEZ IZQUIERDO David[1,b], GAGLIARDI Francesco[1,c], AMBROGIO Giuseppina[1,d], FILICE Luigino[1,e]

[1]University of Calabria, Ponte P. Bucci, cubo 45C, 87036 Arcavacata di Rende (CS), Italy

[a]romina.conte@unical.it, [b]david.rodriguez@unical.it, [c]francesco.gagliardi@unical.it, [d]giuseppina.ambrogio@unical.it, [e]luigino.filice@unical.it

Keywords: Fusion Welding, Finite Element Method, Numerical Analysis

Abstract. Arc welding processes (AWPs) are performed by generating an electric arc between a metal electrode and the workpiece to be joined. Submerged arc welding, belonging to AWPs, is characterized by the peculiarity that the arc is not visible. Indeed, a granular fusible material flux is employed in the process to shield the parts to be processed, avoiding arc radiation and fumes and, at the same time, reducing the oxidation risks of the welded metals. The main process variables are current, voltage and welding speed. These variables have to be properly set to balance the specific heat in the weld pool for a proper process optimization.

Introduction

Fusion welding is a flexible technique characterized by high efficiency [1], widely employed in the mechanical industry to join conventional structural steels. To carry out the process, the materials are heated to a temperature below the melting point and a filler material allows the joint [2].

According to the filler material employed it is possible to distinguish several process variants. One of them is the Submerged Arc Welding (SAW), which the authors focused on. The process principle is based on the generation of an electric arc between the electrode and the base material. The arc is protected by a granular flow of flux from the atmospheric contaminants, in addition it is worth pointing out that the flux itself increases the conduction of the generated arc [3].

During the welding, the involved materials are subjected to heating and cooling phases, which occur very quickly affecting the microstructure creating a new metallurgical condition within the heat affected zone (HAZ) [4,5]. More in detail, the heat input depends on the current, voltage and welding speed, which are the main process parameters to set for carrying out the process. The welding current significantly affects the penetration while the voltage is responsible for the bead width and not greatly contributes to its penetration depth. Therefore, the input process parameters have to be set according to the joint typology and to the thickness of the metals to be joined [3]. The employed energy causes changes at its microstructure and, therefore, at the mechanical properties of the final joint.

The scientific literature reports studies which aim at understanding the influence of the process parameters on the joint. Jou [6] carried out experiments aiming at correlating the main process parameters to the weld bead by numerical investigations in order to predict its size. Numerical analyses and optimization techniques have been widely carried out to predict residual stresses and affected zones in different manufacturing processes [7,8]. These numerical techniques have been employed for analyzing thermal and mechanical behavior of welded components [9] as well as for predicting thermal cycles, residual stresses and deformations induced by this joining method [10]. Other authors reported the numerical simulation of the welding and cooling conditions and the subsequent investigation of the melted zone extension as well as of the HAZ and of the hardness profile [9].

The main focus of this work lies in the setting of a numerical model aiming at analyzing the effect of the variables on a multi-pass welding joint in terms of thermal properties, looking at the characteristics of the bead HAZ and of its distortions and residual stresses.

Material and Method

Material. The material investigated in this study is the medium carbon steel alloy ASTM A516 Grade 70, employed as base material and widely used in the construction of welded pressure vessels. The main requirement for its service is the high notch toughness. The EH14 copper coated wire, generally used in the construction of containers or boilers, was selected as filler material. The following tables (Table 1 and Table 2) report, respectively, the chemical composition and the mechanical properties of the employed materials.

Table 1. Chemical composition of the base and filler material.

	Element [%]					
	C	***Mn***	***P***	***S***	***Si***	***Cu***
ASTM A516 Gr 70	0.31	1.2	0.035	0.035	0.45	-
EH-14	0.10	1.8	0.019	0.013	0.05	0.05

Table 2. Mechanical properties of the base and filler material.

	ASTM A516 Grade 70	**EH-14**
Tensile strength [MPa]	[485-620]	550
Yield strength, min [MPa]	[260]	470
Elongation in 8 in. [200 mm], min, %	17	30
Elongation in 2 in. [50 mm], min, %	21	-

The experimental test, performed to calibrate the heat source, was performed on plates characterized by different thicknesses (Fig. 1a), specifically dimensions of 100×400×10 mm^3 and 100×400×25 mm^3 were welded by SAW employing a specific clamping equipment designed to the aim of this investigation (Fig. 1b).

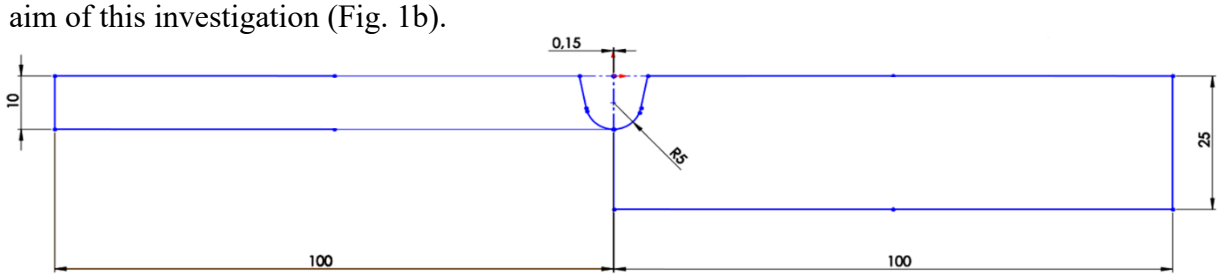

(a)

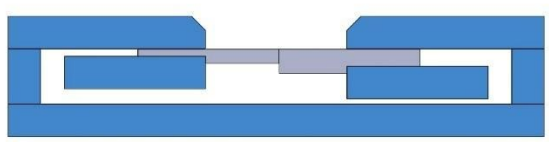

(b)

Fig. 1. a) Coupon geometry (mm) and b) experimental clamping system.

Method. A three-dimensional numerical model was developed by commercial ESI Sysweld software, which is one of the most widely used software for analyzing welding distortions and residual stresses through the finite element method. In fact, the software allows the welding process simulation providing the thermal analysis, which this work focuses on.

The numerical analysis starts with the calibration of the heat source, which characteristics affect the temperature distribution. The heat source moves along the weld path, for each pass taking into consideration specific experimental evidence. The double ellipsoid proposed by Goldak [11,12] was used to the aim of this study and modeled considering as parameters the arc efficiency η, half width of the fused zone a, its penetration depth b, its front length c_f and its back length c_b (Fig. 2).

The numerical model was built by using 80,500 elements and 87,771 nodes. The boundary conditions were defined to replicate the experimental state. This resulted in imposing constraints at a distance of 50 mm from the plates' extremity. Concerning the thermal boundary conditions, an ambient temperature of 20 °C and a heat transfer coefficient ranging from 0.040 to 0.032 W/mm-K, according to the thermal phases of the analyzed material, were set.

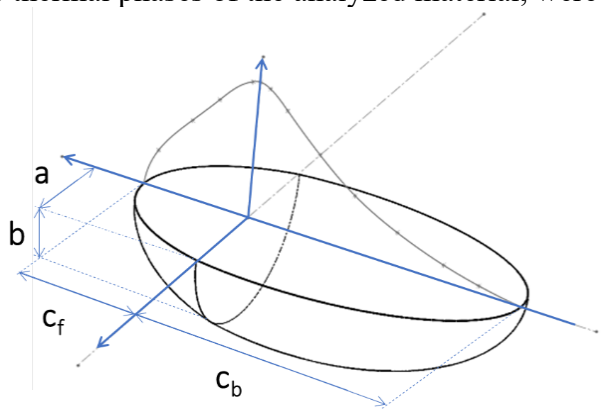

Fig. 2. Goldak's double-ellipsoid and parameters.

A multi-pass welding joint was executed. Specifically, the experimental procedure involves three welding steps. The first one (*Pass 1*) is performed on the bottom side of the plates to be joined and it is aimed at creating a sort of weld cup, while two second passes (*Pass 2*) and all the successive ones (*Pass 3+n*) are performed on the top side, moving on the left and on the right respect to the centerline of the weld bead, until the expected weld bead height is reached. Each pass typology is characterized by a different combination of process parameters and can start just as soon as the temperature measured on the plates is lower than 250°C.

The process parameters considered to the aim of this study are current (I), voltage (V) and welding speed (v). Table 3, below shown, reports the values set for the analyzed case study:

Table 3. Process parameters.

# Pass typology	I [A]	V [V]	v [mm/min]
Pass 1	440	27	320
Pass 2	540	25,4	384
Pass 3+n	675	34	768

Discussion of the Results

The multi-pass welding was investigated by dividing the analysis in two different steps. Specifically, *Pass 1*, being performed on the bottom side of the sheets, was not considered in the analysis. The numerical model starts setting and calibrating *Pass 2* performed in two steps. The first simulation was, therefore, run considering the weld beads obtained experimentally by

overlapping the first two *Pass 2,* hereafter named *Sample A.* To do that, specimens with dimension 70×35×25 mm^3 were firstly cross-sectioned from the center of the test plate and then the surface treated by grinding and polishing and finally etched. Looking at the macrograph (Fig. 4a), each *Pass 2*, and the respective deposit, is clearly visible as well as the HAZ. The geometry of each fused zone, coming from the macrograph, and the process parameters represent the input data for Sysweld. When the process was completely simulated, results were analyzed in terms of temperature distribution (Fig. 4b), comparing the numerical data with the experimental evidence.

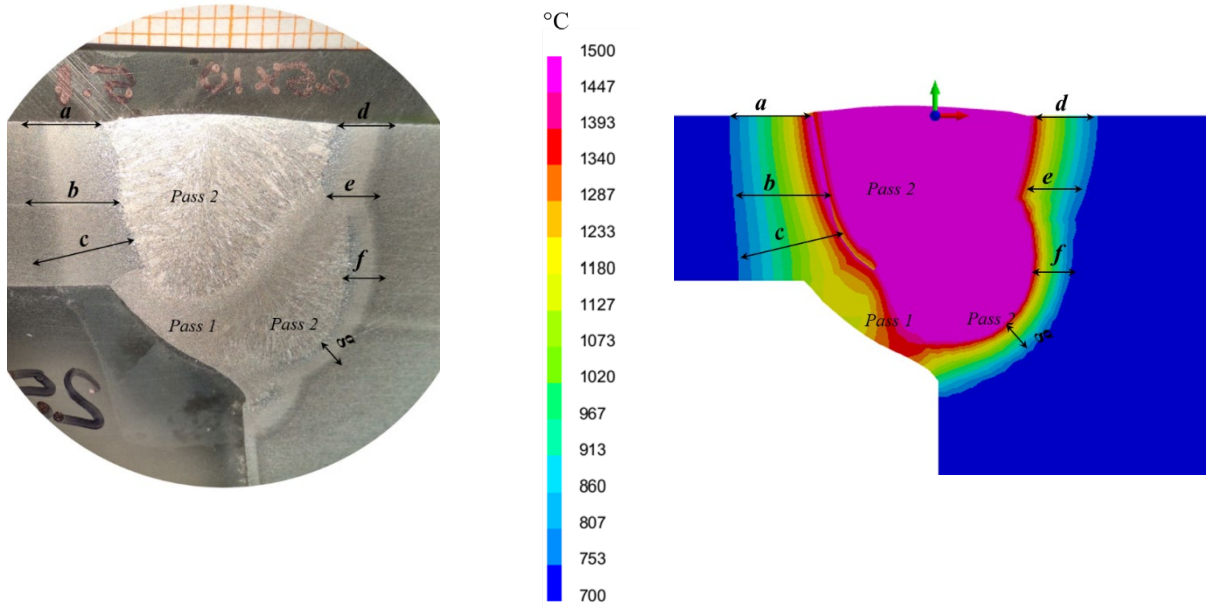

(a) (b)

Fig. 4. HAZ measurement for Sample A: a) experimental test, b) numerical simulation.

In detail, the extension of the HAZ was measured both on the experimental macrograph (five different sections of the same sample were processed) and on the thermal histogram obtained from the simulation. According to that, the upper and lower limits of the temperature scale were set considering, respectively, the beginning of the transition zone in the austenitic field and the melting point of a low carbon steel. For estimating the zone affected by the process temperature, some points were selected and the length defined considering the perpendicular of the tangent to the point. Therefore, the segments a, b, c, d, e, f, g were measured and the values collected for both numerical analysis and experimental test. The comparison of gathered measurements, displayed in Fig. 5, demonstrates that the numerical model was calibrated properly, since the HAZ obtained in *Sample A* is actually equal to the one obtained experimentally.

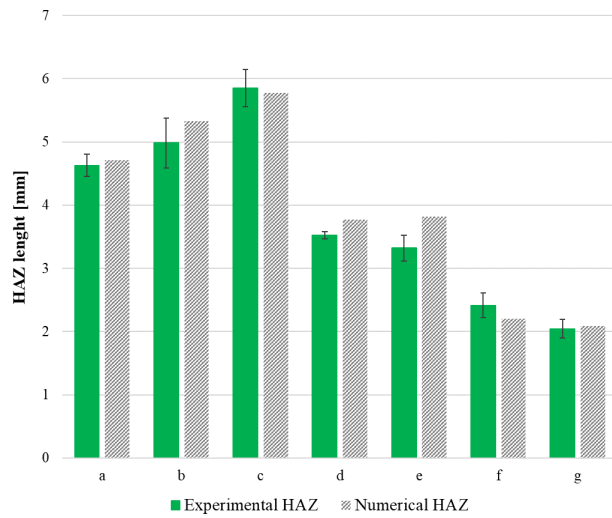

Fig. 5. Sample 1: Comparison of experimental and numerical HAZ lengths.

Once validated the *Pass 2* of the welding sequence, a second joint, hereafter named *Sample B*, was performed overlapping the subsequent *Pass 3+n,* depositing as much as material in order to complete the weld bead, as required by the welding procedure specifications. Two additional welding passes were required, named *Pass 3* and *Pass 4*.

Fig. 6a displays the sectioned joint and each pass can be easily distinguished. It is interesting to look at the 5x enlargement, where the metallurgical transformation, due to the heat influence, of the weld zone, of the heat affected zone and of the base material is observable.

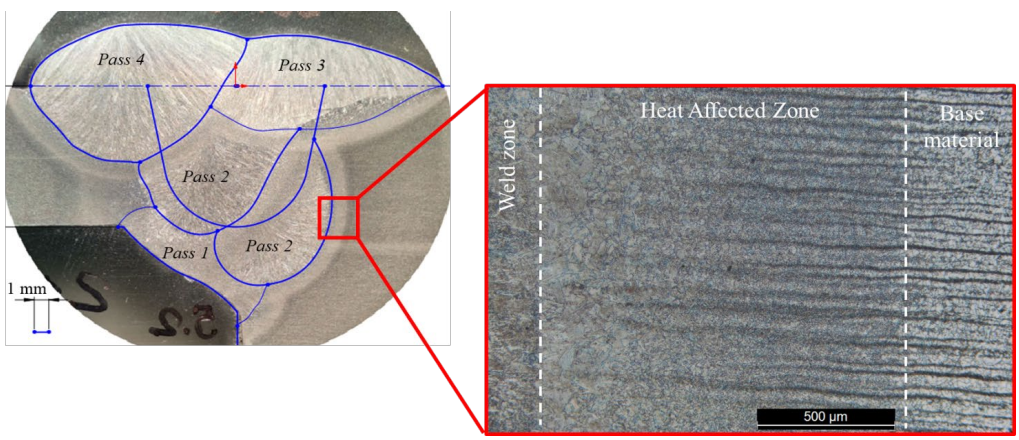

(a) (b)

Fig. 6. a) sectioned view of Sample B and b) its 5x enlargement.

The finite element model was then defined to simulate the welding process on *Sample B*. To be thorough, the measurement of the HAZ was detected as well (Fig. 7), and the comparison between numerical and experimental data, as previously performed for *Sample A*, are synthesized in Fig. 8.

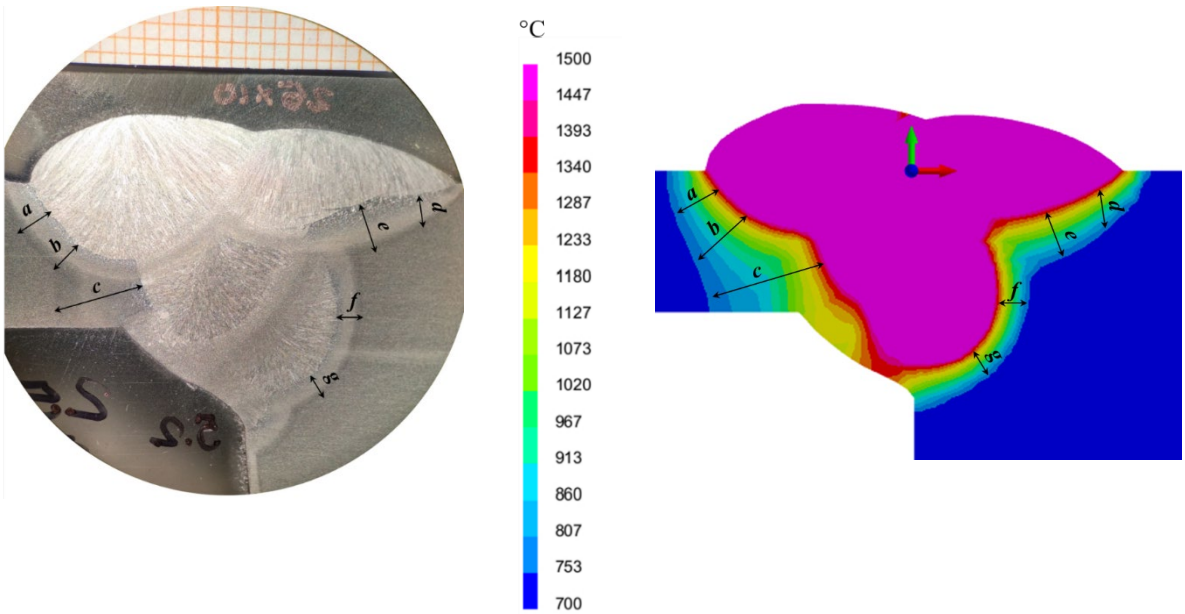

(a) (b)

Fig. 7. Sample B HAZ measurement: a) experimental test, b) numerical simulation.

These further experimental measurements demonstrated the capability of the finite-element simulation in predicting the heat transfer, even if a multi-pass welding is analyzed. The numerical results agree with the experimental data, reasonably. Actually, differences on the left side of the welding bead, especially point *b*, can be detected. The experimental and simulated discrepancies could be attributed to errors related to a possible experimental variance along the length of the weld bead, considering also that the dimension of the samples is far from the usual industrial standards and, therefore, steady-state conditions could be just partially reached. Anyway, additional analyses are required to explain the highlighted inaccuracy, more clearly.

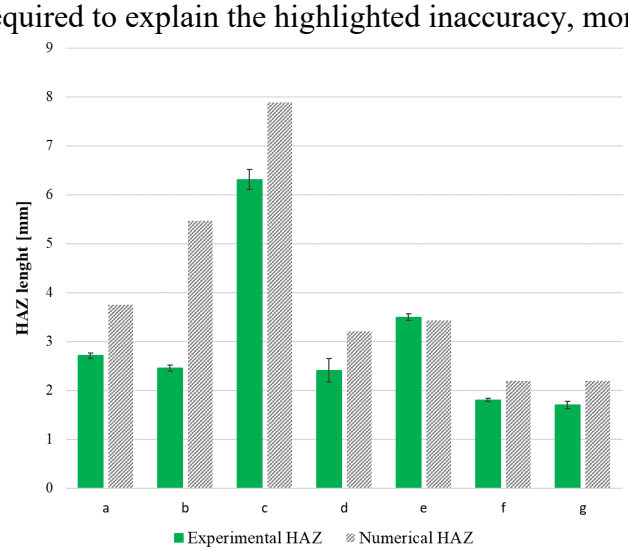

Fig. 8. Sample B: Comparison of experimental and numerical HAZ lengths.

The experimental and numerical comparison proved the effectiveness of the numerical model therefore the potentiality of the obtainable results in improving the performance of jointed parts can be deduced by looking at displacements and residual stresses generated on the parts owing to

the multi-pass welding. Herein, for example, the dishomogeneity related to the different thicknesses of the sheets to be welded are observable, clearly (Fig. 9). Practically, this information can be useful to set a different clamping system and/or welding sequence to compensate for unbalanced stress and strain distributions, important for easier parts' assembly and for their fatigue life behavior.

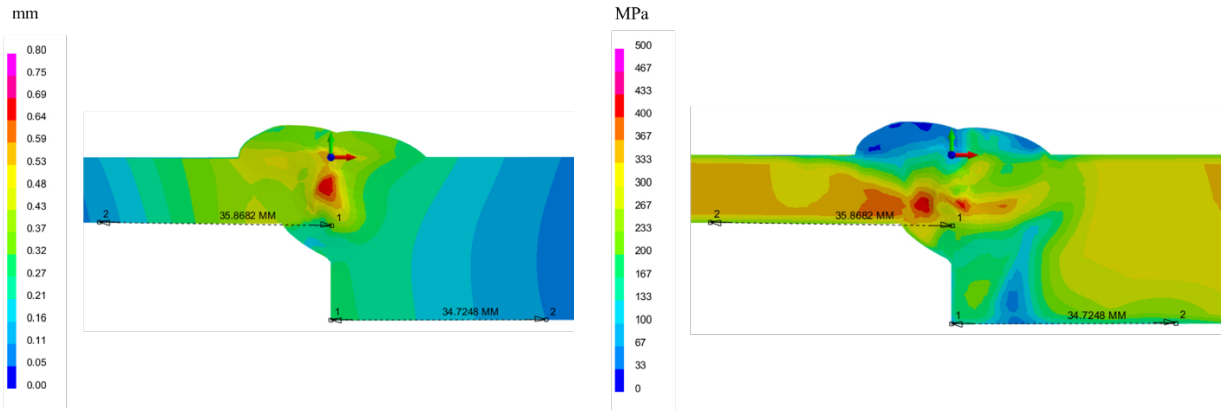

(a) (b)

Fig. 9. a) Displacement and b) residual stress on Sample B at the end of the welding process.

Summary

In this work, the temperature distribution, the distortions and the residual stress within multi-pass welding of plates, characterized by different thickness, were investigated by a finite element simulation properly calibrated by experimental evidence. Specifically, the geometric parameters of the double Goldak's ellipsoid were set and applied on specific positions of the weld beads' geometry extracted by each experimental welding pass. The adjustments of heating source's shape, efficiency and position were performed to achieve a conformity between temperature distribution, obtained by the numerical analysis, and extension of the HAZ, extracted by micrographs of sectioned and prepared samples.

The obtained results showed a good overlap between the numerical and the experimental results, therefore, considering the good calibration of the model, preliminary results on distortions and residual stresses, difficult to analyse experimentally, where observed. Further analyses will be carried out by comparing, in terms of HAZ, distortions and residual stress, more samples processed by different process parameters, in order to speed the welding optimization up.

References

[1] R. Singh, Applied welding engineering: processes, codes, and standards., Butterworth-Heinemann, 2020.

[2] J.A. Schey, Introduction to Manufacturing Processes, 3rd editio, McGraw-Hill Higher Education, 2000.

[3] A. Singh, R.P. Singh, A review of effect of welding parameters on the mechanical properties of weld in submerged arc welding process, Mater. Today Proc. 26 (2020) 1714-1717. https://doi.org/10.1016/j.matpr.2020.02.361

[4] M. Zhang, Y. Han, C. Jia, Z. Zheng, H. Li, C. Wu, Improving the microstructures and mechanical properties with nano-Al2O3 treated wire in underwater submerged arc welding, J. Manuf. Process. 74 (2022) 40-51. https://doi.org/10.1016/j.jmapro.2021.11.056

[5] G. Labeas, I. Diamantakos, Numerical investigation of through crack behaviour under welding residual stresses, Eng. Fract. Mech. 76 (2009) 1691-1702. https://doi.org/10.1016/j.engfracmech.2009.03.006
[6] M. Jou, Experimental Investigation of Resistance Spot Welding for Sheet Metals Used in Automotive Industry., JSME Int. J. Ser. C. 44 (2001) 544-552. https://doi.org/10.1299/jsmec.44.544
[7] Z. Pu, D.Umbrello O., W. Dillon Jr, Jawahir S., Finite Element Simulation of Residual Stresses in Cryogenic Machining of AZ31B Mg Alloy, Procedia CIRP 13 (2014) 282-287. https://doi.org/10.1016/j.procir.2014.04.048
[8] G. Rotella, S. Rinaldi, L. Filice, Roller burnishing of Ti6Al4V under different cooling/lubrication conditions and tool design: effects on surface integrity, Int. J. Adv. Manuf. Tech. 106 (2020) 431-434. https://doi.org/10.1007/s00170-019-04631-z
[9] H.M.E. Ramos, S.M.O. Tavares, P.M.S.T. de Castro, Numerical modelling of welded T-joint configurations using SYSWELD, Sci. Technol. Mater. 30 (2018) 6-15. https://doi.org/10.1016/j.stmat.2018.08.002
[10] G. Romaní, A. Portolés, Modelo tridimensional de simulación por MEF para estudiar la influencia de variables esenciales de soldadura robotizada GMAW en uniones a tope planas., Sold. y Tecnol. Unión. 19 (2008) 22-26.
[11] J. Goldak, A. Chakravarti, M. Bibby, A new finite element model for welding heat sources, Metall. Trans. B. 15 (1984) 299-305. https://doi.org/10.1007/BF02667333
[12] J.H. Chujutalli, M.I. Lourenço, S.F. Estefen, Experimental-based methodology for the double ellipsoidal heat source parameters in welding simulations, Mar. Syst. Ocean Technol. 15 (2020) 110-123. https://doi.org/10.1007/s40868-020-00074-4